Temperature-induced band gap renormalization in Mg_2Si and Mg_2Sn

Wenliang Yao,[1,*] Bowen Shi,[1,2,*] Shunbo Hu,[1,3,†] Peng Zhang,[1] Jinyang Xi,[1,‡] Yin Wang,[1,4] David J. Singh,[5] and Wei Ren[1,§]

[1]*Physics Department, Institute for the Conservation of Cultural Heritage, Materials Genome Institute, International Center for Quantum and Molecular Structures, Shanghai University, Shanghai 200444, China*

[2]*Shanghai World Foreign Language Academy, 400 Baihua Street, Shanghai 200233, China*

[3]*Key Laboratory of Silicate Cultural Relics Conservation (Shanghai University), Ministry of Education, Shanghai 200444, China*

[4]*Hongzhiwei Technology (Shanghai) Co., Ltd., Shanghai 201206, China*

[5]*Department of Physics and Astronomy, University of Missouri, Columbia Missouri 65211, USA*

(Received 22 February 2023; revised 5 September 2023; accepted 9 October 2023; published 30 October 2023)

$Mg_2Si_{1-x}Sn_x$ solid solutions show enhanced thermoelectric performance due to band convergence, especially when the x is approximately 0.7. The complex band edges arising from crossover of two conduction bands have been discussed from various aspects, but the temperature-induced band edges renormalization have been neglected. We report the electron-phonon renormalization in Mg_2Si and Mg_2Sn and find different responses of band gap with temperature. The contributions from lattice expansion and temperature induced atomic vibrations are both considered. The band gaps of the end-point compounds are found to have opposite temperature dependences (e.g., from 0 to 800 K, the Mg_2Si gap decreases by ∼0.12 eV while the Mg_2Sn gap increases by ∼0.02 eV). The remarkably different temperature dependences are due to the different chemical characters of the two conduction bands (light and heavy bands) in Mg_2Si and Mg_2Sn. Our work reveals the origin of relationship between temperature and electronic structure of the band edges in Mg_2Si and Mg_2Sn. This behavior extends to the alloy system. The temperature effect does not affect the result that there is band convergence of the two carrier pockets near the conduction band minimum in the Mg_2(Si, Sn) alloy thermoelectric system.

DOI: 10.1103/PhysRevB.108.155205

I. INTRODUCTION

Thermoelectric (TE) materials enable direct conversion between thermal and electrical energy. Among other applications, they enable conversion of waste heat into useful electricity. This is a topic of great interest for energy technology [1–4], but is limited by the conversion efficiency possible with existing thermoelectric materials. The TE conversion efficiency is limited by the figure of merit, $ZT = S^2\sigma T/\kappa$ of the materials. Here T is the temperature, S is the Seebeck coefficient, σ is the electrical conductivity, and κ is the thermal conductivity. In order to obtain large ZT, increasing the power factor ($S^2\sigma$) and/or reducing the thermal conductivity is necessary. However, the optimization of TE performance is challenging because of the counter-correlations of the transport parameters entering ZT [5]. Strategies that have been used to overcome this include the "phonon glass electron crystal" concept [6], the use of nanostructuring [7], and various band engineering approaches [4,8–10]. The solid solution, $Mg_2Si_{1-x}Sn_x$ is of particular interest due to the high TE conversion efficiency that is obtained for n-type samples at certain compositions, x, as well as the practical advantages of relatively low cost, nontoxicity, and stability [11–16]. Mg_2Si and Mg_2Sn are indirect band gap semiconductors with two low-lying conduction bands [the lower mass (C_L) and higher mass (C_H) bands]. The order of minima of these two bands is opposite in the two compounds. The lowest conduction band minimum is C_L in Mg_2Si and C_H in $MgSn_2$. Consequently, for some composition x, the $Mg_2Si_{1-x}Sn_x$ solid solution displays a convergence in energy, where the two conduction band minima differ in energy by less than $2k_BT$ [13]. It has been argued that the resulting increased valley degeneracy leads to a significantly enhanced density-of-states effective mass, which gives rise to enhanced Seebeck coefficients for a given carrier density and consequently enhanced power factor and thermoelectric performance [13]. This is supported by experimental results showing high performance of $Mg_2Si_{1-x}Sn_x$ solid solutions in this composition range, where an optimized ZT of 1.3 for $x \approx 0.7$ at 700 K has been obtained in experiments [13]. However, while the alloy composition is key to this band convergence, there may be other important factors influencing the band structure and band convergence [17–19]. Here we show that temperature is crucial for understanding band convergence due to the very different temperature dependences of the light and heavy bands involved in this system.

Theoretically, there are two main sources of temperature dependence of the band structure. These are the lattice thermal expansion and the electron-phonon interaction, whereas the change of electronic structure caused by phonon vibrations is called the electron-phonon renormalization (EPR) [20–24], which includes both the effect of thermally populated phonons and zero-point vibrations. A well-known effect in

*These authors contributed equally to this work.
†shunbohu@shu.edu.cn
‡jinyangxi@t.shu.edu.cn
§renwei@shu.edu.cn

semiconductor physics, redshift or blueshift of the gap with temperature is often referred to as the Varshni effect or inverse Varshni effect [18,22,25–34]. This has been studied theoretically from the Allen-Heine-Cardona theory with a "one shot" method [35–37]. For example, Zhang *et al.* have reported the temperature-dependent band gaps in some classical covalent and ionic semiconductors [38]. The band gaps of diamond, Si, SiC, MgO, and NaCl generally decrease at high temperature [33,34,38]. On the contrary, the band gap in $Ge_2Sb_2Te_5$ increases with temperature [28]. Prior work has noted the possible importance of temperature in certain TE materials [18,19,22,27,28,37,39–44], such as PbTe [19], SnTe [43], and $CoSb_3$ [42]. Those results show that the band convergence may affect the thermoelectric behavior of these materials at high temperatures. For example, D'Souza and Querales-Flores *et al.* investigated temperature dependent alignment of the L and Σ valleys in PbTe [18,44].

Here we explore the temperature dependent changes of in the band structures of Mg_2Si, Mg_2Sn and $Mg_2Si_{1-x}Sn_x$ solid solutions, finding that these are important for understanding the TE properties. We study and decompose the EPR effect on band structures of Mg_2Si, Mg_2Sn and $Mg_2Si_{0.375}Sn_{0.625}$. We do this using a recently developed one-shot method for calculating EPR [20]. In the case of Mg_2Si, the band gap decreases with temperature, while that of Mg_2Sn increases weakly. The band convergence is governed by the relative positions of the light and heavy conduction band minima. This is affected by both temperature and lattice constants. The results confirm that temperature does not change the fact that there is a convergence between C_L and C_H in the solid solution near a composition of $Mg_2Si_{0.375}Sn_{0.625}$, but do indicate that temperature dependent shifts should be considered in relation to interpreting data on this system.

II. METHODS

We investigate EPR effect at finite temperatures by using the quasiharmonic approximation (QHA) and the "one-shot" method [20]. The procedure used is as follows: (1) The temperature dependent structures were determined using the QHA, in particular to obtain the volume (V) as a function of temperature [45]. (2) The phonon spectra were calculated using $4 \times 4 \times 4$ supercells with the temperature dependent structures $V(T)$. (3) The one-shot method was used where atoms are displaced from their equilibrium positions by $\Delta\tau$, based on the phonons and Gaussian widths due to the T dependent phonon occupations as given in [20]. (4) The effective band structure (EBS) at T is predicted by unfolding the band energies in the supercell into the primitive cell.

The present work is based on first-principles density functional calculations. These are performed using the Vienna *ab initio* Simulation Package (VASP) [46–48], with standard settings. The projector augmented-wave method is applied with a plane wave cutoff energy of 520 eV [49]. The generalized gradient approximation (GGA) of the Perdew-Burke-Ernzerhof (PBE) type is used as the exchange-correlation functional [50] for total energy calculations as needed for the phonons. The electronic structures are calculated by using the modified Becke-Johnson (mBJ) meta–GGA potential [51,52]. This is important for improving the accuracy of band gap prediction in relation with experiment. We use the mBJ potential for both the band structures and the one-shot calculations for the temperature dependent band shifts. The energy convergence accuracy is 10^{-8} eV. To obtain the optimized structure with sufficient stability for phonon calculations, the convergence criterion for the force acting on atoms is 10^{-5} eV/Å. A $4 \times 4 \times 4$ supercell (192 atoms) and the corresponding $4 \times 4 \times 4$ supercell (192 atoms) with $2 \times 2 \times 2$ Monkhorst-Pack **k** grids are used for quasiharmonic approximation (QHA) and the "one-shot" method [20] calculations, respectively. In addition, a $2 \times 2 \times 2$ supercell as in Fig. S1 of the Supplemental Material [53] and $2 \times 2 \times 2$ Monkhorst-Pack **k**-grids were used for QHA and "one-shot" calculations, respectively, for the $Mg_2Si_{0.375}Sn_{0.625}$ composition. Phonon calculations were performed using a supercell approach. Real-space force constants were calculated in the density-functional perturbation theory implemented in the VASP code for Mg_2Si and Mg_2Sn. In order to improve the computational efficiency, the phonon spectrum of $Mg_2Si_{0.375}Sn_{0.625}$ was obtained by using the PHONOPY code based on the finite differences method [45]. The results of the two methods match very well as shown in Fig. S2 in the Supplemental Material [53].

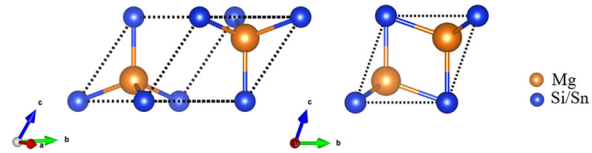

FIG. 1. Crystal structure of the primitive cell of Mg_2Si and Mg_2Sn, yellow and blue spheres are Mg and Si/Sn atoms, respectively.

Finally, we note that the one-shot calculations that we do are based on the adiabatic approximation. This approximation, while common, has limitations, and in particular it has been noted that there can be a significant error for the zero point renormalization for polar semiconductors [37,54,55]. Prior reports of the lattice dynamics indicate a substantial ionic component reflected in Born charges somewhat lower than but close to the nominal charges of +2 and -4 for Mg and Si, respectively, in Mg_2Si [56,57]. The error in the adiabatic approximation is related to the long-range Coulomb interaction. While we are unable to quantify nonadiabatic corrections for Mg_2Si and Mg_2Sn, we expect that these contributions are not dominant, especially considering the relatively high dielectric constant, which is approximately 20 in Mg_2Si [58].

III. RESULTS AND DISCUSSION

The antifluorite-type compounds Mg_2Si and Mg_2Sn are shown schematically in Fig. 1. These are semiconductors, with eight valence electrons per formula unit and as mentioned, the n-type alloy, $Mg_2Si_{1-x}Sn_x$ is a well-known TE material [59,60]. They have space group Fm-$3m$ and are indirect band gap semiconductors. The primitive cells contain the Mg and Si (Sn) atoms located at the 8c: (0.25, 0.25, 0.25) and 4a: (0, 0, 0) sites, respectively. The lattice constants of Mg_2Si and Mg_2Sn using the PBE functional are 6.35 Å and 6.81 Å, respectively. These values are very close to the experimental values [61]. Temperature dependence $V(T)$ and volumetric

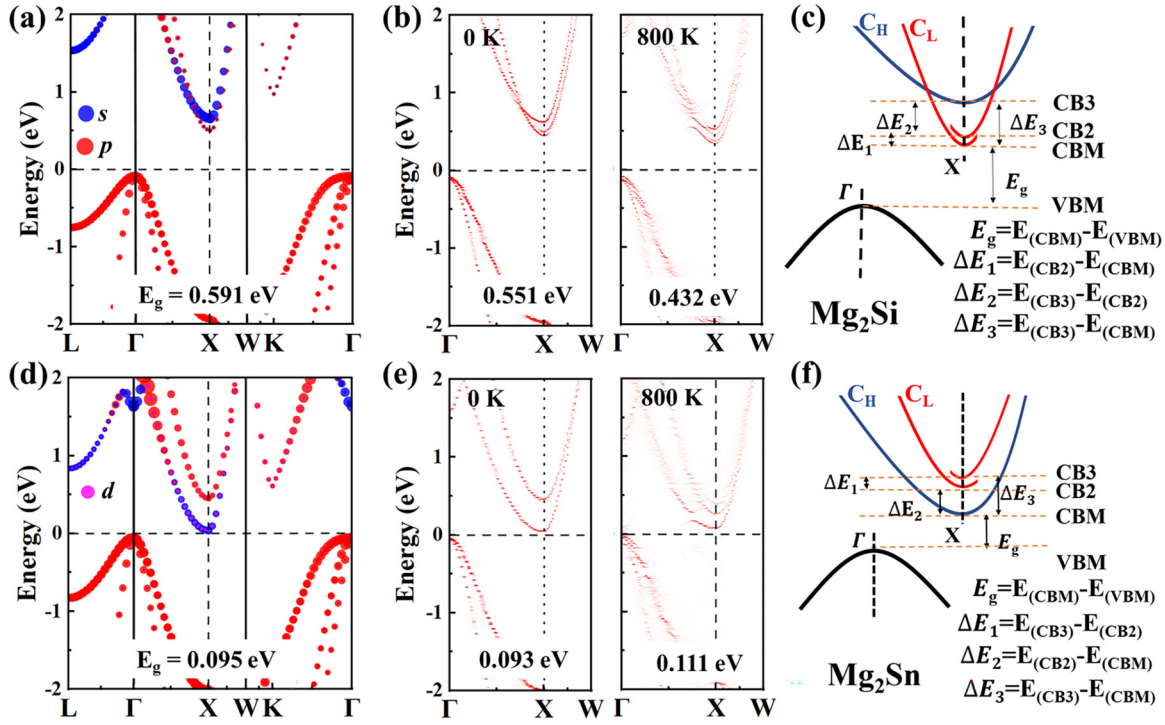

FIG. 2. The projected (mBJ) band structures of (a) Mg_2Si and (d) Mg_2Sn primitive cells, as well as the EBSs at 0 and 800 K for (b) Mg_2Si and (e) Mg_2Sn, respectively. The schematic diagram for the band structure identification for (c) Mg_2Si and (f) Mg_2Sn. The Fermi energy is set as the zero of energy and the high-symmetry points are **L** (0.5 0.5 0.5), **Γ** (0 0 0), **X** (0.5 0 0.5), **W** (0.5 0.25 0.75), **K** (0.375 0.375 0.75). The size of the colored dots indicates the weights of different orbitals.

expansion coefficient α_V from 0 to 800 K are obtained by the QHA method and shown in Fig. S3 of the Supplemental Material [53]. The α_V results of Mg_2Si and Mg_2Sn are typical of common compounds (e.g., at 300 K, 5.305×10^{-5} K^{-1} for Mg_2Si, 6.238×10^{-5} K^{-1} for Mg_2Sn).

The electronic band structures of Mg_2Si and Mg_2Sn primitive cells without EPR are shown in Figs. 2(a) and 2(d). Figures 2(b) and 2(e) show the band structures with EPR for Mg_2Si and Mg_2Sn at 0 K and 800 K, respectively. The mBJ potential was used for these band structure calculations. Both compounds show an indirect gap with conduction band minima along the **X**−**Γ** direction. The indirect band gap values of Mg_2Si and Mg_2Sn are calculated to be 0.591 and 0.095 eV, which are somewhat lower than quoted literature values of 0.69–0.78 eV for Mg_2Si and 0.23–0.33 eV for Mg_2Sn, respectively [61–63]. We show the projected band structures without EPR of Mg_2Si and Mg_2Sn in Figs. 2(a) and 2(d). The schematic diagram for the band structure identification for Mg_2Si and Mg_2Sn in Figs. 2(c) and 2(f), respectively [64]. The C_L is shown in red, and the blue represents the C_H for Mg_2Sn and Mg_2Si [17] (the EBSs in two materials between 0 and 800 K are given in the Figs. S4 and S5 of the Supplemental Material [53]). Importantly, two conduction bands corresponding to C_L and C_H are reversed in order between Mg_2Si with Mg_2Sn. The lowest-lying band is the light band (C_L) in Mg_2Si, and it is the heavy band (C_H) for Mg_2Sn. This is the basis for the band convergence in the alloy system [13]. The C_L of Mg_2Si is mainly contributed by Mg-*p* and Si-*s* orbitals, while the C_H band comes from the Mg-*s* orbital, as seen in Fig. 2(a). Similarly, the C_L band Mg_2Sn is mainly contributed by Mg-*p*, Sn-*s*, and Sn-*d* orbitals, while the C_H band has Mg-*s* and Sn-*d* orbitals character. Both the C_H and C_L pockets are triple degenerate at the X point, in the sense that there are six equivalent half-pockets in the Brillouin zone at the six equivalent X points. These pockets, specifically the CBM and CB3 pockets, are not band degenerate at a given single X point. The band edges at the VBM in Mg_2Si (Mg_2Sn) are contributed by Si-*p* (Sn-*p*) orbitals. It is noteworthy that the C_L splits in the one shot EPR calculation. This reflects the effect of the frozen in atomic displacements that break symmetry, and in this sense the splitting is an artifact of the calculation. It is, however, of interest since it reflects the strength of the EPR [65].

In the schematic diagram is shown the identification of the valence band maximum (VBM), the conduction band minimum CBM, the second conduction band (CB2), and the third conduction band (CB3) in the band structure with EPR for Mg_2Si and Mg_2Sn. The two split energy levels of C_L for Mg_2Si are marked by CBM and CB2, whereas the C_L splits in Mg_2Sn are denoted by CB2 and CB3, respectively. The difference between C_L and C_H qualitatively reflects different electron-phonon couplings for the two pockets, in particular that the EPR effect is stronger for C_L reflecting its different orbital character from C_H.

The electronic structure shown in the EBS is influenced by the EPR including band gap changes with temperature and zero-point renormalization (ZPR) [66]. The ZPR is defined by the value of $E_g(T = 0) - E_g(\text{static})$. From Fig. 2, we find ZPR values for Mg_2Si and Mg_2Sn of −0.040 eV and −0.002 eV, respectively. Table I summarized ZPR for Mg_2Si, Mg_2Sn and

TABLE I. Band gaps (in eV) for Mg_2Si, Mg_2Sn and $Mg_2Si_{0.375}Sn_{0.625}$ at different temperatures. These values are extracted from the EBSs with the consideration of EPR.

Temperature (K)	Mg_2Si Indirect Gap	Mg_2Sn Indirect Gap	$Mg_2Si_{0.375}Sn_{0.625}$ Direct Gap
ZPR	−0.040	−0.002	−0.025
Without EPR	0.591	0.095	0.286
0	0.551	0.093	0.261
100	0.546	0.103	0.246
200	0.536	0.102	0.251
300	0.516	0.105	0.236
400	0.495	0.121	0.204
500	0.482	0.147	0.216
600	0.472	0.144	0.184
700	0.453	0.148	0.165
800	0.432	0.111	0.101

$Mg_2Si_{0.375}Sn_{0.625}$. The ZPR for Mg_2Si is remarkable, while it has a very small value for Mg_2Sn. This is partly because the heavier Sn atoms have smaller zero-point displacements as also reflected in the lower frequency phonons in that material and it is also partly due to the different bands making up the conduction band minimum. The ZPR is distinct from the high temperature behavior, which is governed primarily by force constants as opposed to the mass. This is a consequence of equipartition at higher temperature. For the phonons, the lattice expansion (LE) at finite temperature has greater influence on the optical branches, and the phonon modes are softened at higher temperature from the phonon spectra at 0–800 K. We find no imaginary phonons in Mg_2Si and Mg_2Sn. This allows the EPR calculations based on the QHA method. The phonon spectra of Mg_2Si and Mg_2Sn are shown in the Figs. S6 and S7 of the Supplemental Material [53]. These include the effect of zero-point motion.

Interestingly, with temperature increase, the trends in the E_g change due to EPR are opposite for Mg_2Si and Mg_2Sn. For instance, the reduction of E_g is ∼0.119 eV from 0 to 800 K for Mg_2Si. On the contrary, the E_g is increased by ∼0.018 eV for Mg_2Sn. This dependence of E_g at fine temperature is considered both lattice expansion and lattice vibrations (LE+VIB). Further, we individually calculated the EBSs considering only LE, and only lattice vibration (VIB). The resulting values for LE or VIB are shown in Fig. 3(a). For the calculations with only the vibration effect, the vibration results (frequencies, eigenvectors) are firstly calculated based on the 0 K lattice parameters without the lattice expansion. Then, the vibration-induced atomic positions at given temperature are set for the "one-shot" method while the lattice parameters are fixed at the 0 K values. Thus, the structure at T only including the atomic vibrations is obtained and the band gap calculated as usual in the one shot method. Considering only the lattice expansion, the band gap of Mg_2Si increases monotonically, while oppositely to that of Mg_2Sn which decreases monotonically. This is consistent with previous studies on the variation of conduction band under strain [17,67]. Turning to the vibrational effect, the band gaps of Mg_2Si affected only by VIB decreases monotonically, while again that of Mg_2Sn behaves oppositely and increases monotonically. The results as given in Fig. 3(a) show VIB effect is more significant than LE. Consequently, the combined LE+VIB effects are dominated by the VIB. This is similar to what was reported in the oxide TiO_2 [30]. The important conclusion is that the bands (C_H and C_L) shift by the LE are against to VIB in the two materials with temperature. The band structures as influenced by LE, VIB, and LE+VIB for Mg_2Si and Mg_2Sn are shown in Figs. S4 and S5 and S8–S11, of the Supplemental Material [53].

The absolute energy levels for the C_L (CBM-Mg_2Si, CB3-Mg_2Sn), C_H (CB3-Mg_2Si, CBM-Mg_2Sn), and VBM as functions of temperature reflect the different temperature dependent shifts of the C_L and C_H as shown in Fig. 3(b). Figure 3(b) demonstrates that the C_L and C_H have a similar renormalization trend in Mg_2Si and Mg_2Sn. The average value of the 1s core level of Mg atom is used as the reference,

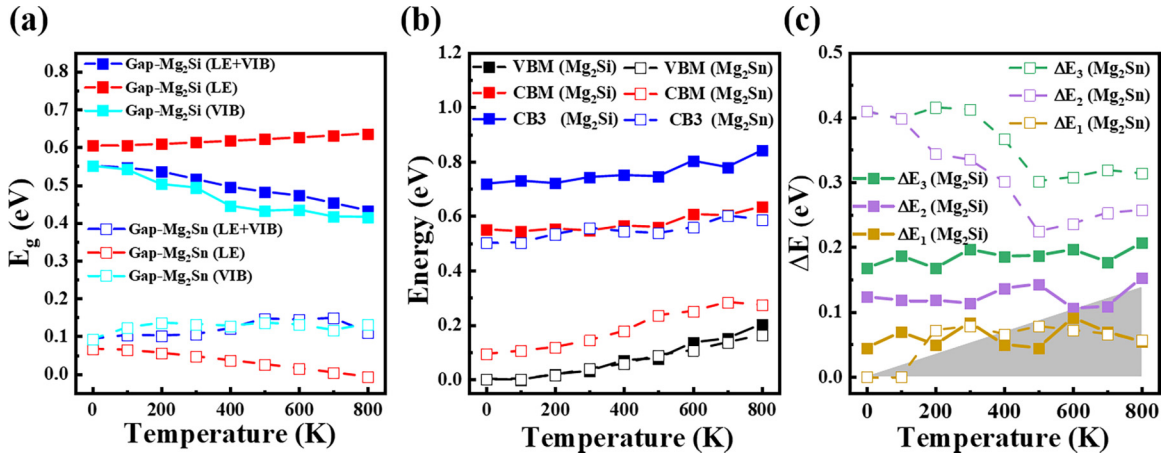

FIG. 3. (a) The temperature dependence of the band gap including only the LE or VIB effect and the combined effect of LE+VIB is shown in red, cyan, and blue, respectively. (b) The absolute energy levels for the VBM (black), CBM (red) and CB3 (blue) as functions of temperature. (c) The energy difference of ΔE_1, ΔE_2 and ΔE_3 with (LE+VIB) effects at different temperatures. The gray area represents a Fermi distribution width of $2k_BT$. The solid square and solid line represent Mg_2Si, while the open squares and corresponding line represents Mg_2Sn.

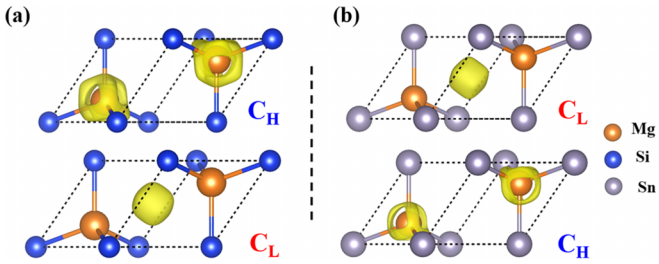

FIG. 4. The band-decomposed charge density plots of C_L and C_H are shown in Mg_2Si(a) and Mg_2Sn(b), respectively.

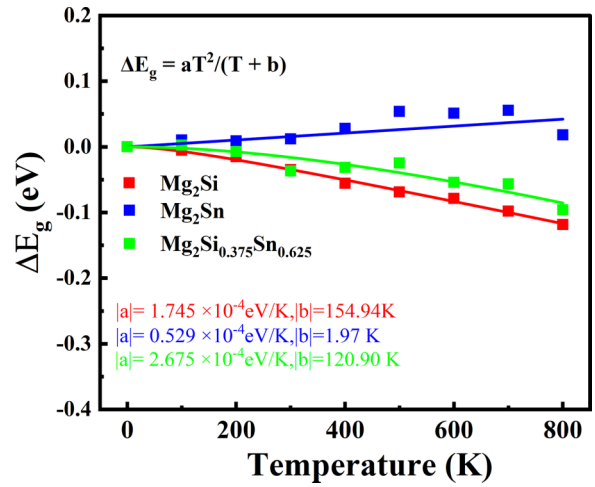

FIG. 5. The temperature-dependence gap of Mg_2Si (red), Mg_2Sn (blue), $Mg_2Si_{0.375}Sn_{0.625}$ (green) with the corresponding nonlinear fittings by the Varshni equation of $\Delta E_g = aT^2/(T + b)$. The absolute values of coefficients $|a|$ and $|b|$ are listed, and the band gaps at 0 K are set as the references.

and the energy of VBM at 0 K is set as zero. According to the absolute energy levels, we find that the change of band gap by the EPR is due to the different responses of CBM and VBM energy levels. The energy levels of VBM of Mg_2Si (black solid square) and Mg_2Sn (black open square) both shift up with the similar trends. For CBM, the energy level of Mg_2Sn (C_L of red open square) moves up, but that of Mg_2Si (C_H of red solid square) changes very insignificantly. Therefore, the band gap for Mg_2Si shows a stronger temperature dependence. In addition, it may be noted that the smaller magnitude of the bare band gap in Mg_2Sn compared to Mg_2Si may play an important role in enhancing the contribution of the valence bands to the CBM renormalization via hybridization.

In addition, we extract the variation of the different energy levels that is ΔE_1, ΔE_2, and ΔE_3, which reflect the degree of degeneracy with EPR in Fig. 3(c). The ΔE_1 represents the energy level splitting, and becomes smaller than $2k_BT$ above 400 K thus contributing favorably to degeneracy. The ΔE_2 and ΔE_3 shown the energy difference between the C_H and C_L varies very little with temperature, which do not obviously affect the band convergence. We additionally studied the EBS in the alloy $Mg_2Si_{0.375}Sn_{0.625}$, which is close to the optimal solid solution composition from experiment, with a supercell. We can find the band gap decreases, and temperature does not change the fact that there is convergence of the light and heavy bands. The bands still converge at high temperature because the band edge shifts by LE and VIB are opposite which results in offsetting each other. These results shown in Figs. S12–S14 of the Supplemental Material [53] show the LE+VIB effects, while as expected the phonon spectra as given in Fig. S15 confirm the structural stability. Combined with LE+VIB, VIB plays a major role in band structure dependence, which needs to be considered.

As mentioned above, the behaviors of band gap with temperature can be attributed to the different dependence of C_H and C_L on temperature. In order to elucidate the relationship with the orbital characters, we visualize the decomposed charge density distribution of C_H and C_L at X points for Mg_2Si and Mg_2Sn in Figs. 4(a) and 4(b), similar to prior analysis [59,68]. Then, we find that the band-decomposed charge density distribution of C_H surrounding the Mg atom significantly results in electronic states that strongly couple to atomic vibrations. The C_L charge density is very local in the central cavity of the structure [68], which is distinct from C_H and weakly effected by lattice vibration. This provides a qualitative explanation for the different behaviors of the renormalization magnitude of the CBM and CB3 bands displayed in Fig. 3(b) in Mg_2Si and Mg_2Sn.

It is of particular interest that the temperature dependence of band gap can be fitted by Varshni equation $\Delta E_g(T) = aT^2/(T + b)$. The variations of band gap for Mg_2Si, Mg_2Sn and $Mg_2Si_{0.375}Sn_{0.625}$ are extracted from their band structures with the consideration of EPR and plotted as function of temperature in Fig. 5 (the band gap at 0 K is set as the reference). The EBSs for $Mg_2Si_{0.375}Sn_{0.625}$ are shown in Figs. S17 and S18 of the Supplemental Material [53]. Here, $\Delta E_g(T)$ is the band gap difference between at temperature T and at 0 K in Fig. 5. Meanwhile, the coefficients $|a|$ and $|b|$ can be obtained. Especially, the larger absolute value of $|a|$ represents $\Delta E_g(T)$ changing with T more strongly, and the smaller $|b|$ shows a more linear relationship between $\Delta E_g(T)$ and T. The absolute values of $|a|$ are 1.745, 0.529, 2.675×10^{-4} eV/K^{-1} for Mg_2Si, Mg_2Sn, $Mg_2Si_{0.375}Sn_{0.625}$. It is perhaps surprising that the temperature dependence of the fitting parameter for the band gap of $Mg_2Si_{0.375}Sn_{0.625}$ is nearly the same as that for Mg_2Si even though the composition is much closer to that of Mg_2Sn in Fig. 5. However, it is important to note that the temperature dependence of the fitting parameter for the band gap mainly depends on the relative position of energy level between CBM (C_L or C_H) and VBM for Mg_2Si, Mg_2Sn, respectively, shown in Fig. 2. Thus, there are two aspects: the individual temperature dependences and the relative positions. Theoretically, when $x \leqslant 0.625$ of $Mg_2Si_{1-x}Sn_x$, the temperature dependence of the band gap are similar to Mg_2Si due to the band gap controlled by CBM (C_H) and VBM [13].The temperature influences convergence of the conduction bands including mainly two parts of lattice vibration and lattice expansion. The results of considering lattice expansion show that C_H and C_L in $Mg_2Si_{0.375}Sn_{0.625}$ do not degenerate at high temperature in Fig. S12 of the Supplemental Material [53]. However, the C_H and C_L remain degenerate at high temperatures after considering lattice vibration as shown in Fig. S14 of the Supplemental Material

[53], which is helpful to improve the density of states and the thermoelectric performance. In conclusion, the results of our calculated temperature-dependent band gap shall have a guiding significance for experiments of Mg_2Si, Mg_2Sn and $Mg_2Si_{0.375}Sn_{0.625}$. In general, the EPR effect is found to be dominant and not negligible at finite temperature.

IV. CONCLUSION

In this paper, we have applied electron-phonon renormalization theory to calculate the different responses of temperature-induced band gap change for Mg_2Si, Mg_2Sn and $Mg_2Si_{0.375}Sn_{0.625}$, in which the contributions from LE and VIB are both considered at finite temperatures. By comparing the contributions of LE and VIB on the band gap of Mg_2Si and Mg_2Sn, we reveal that they have opposite effects. The remarkably different temperature dependences are understood by the distinct characteristics of the two conduction bands (C_H and C_L) in Mg_2Si and Mg_2Sn. Furthermore, from 0 to 800 K, temperature does not obviously affect band convergence in the alloy at the particular composition of $Mg_2Si_{0.375}Sn_{0.625}$, where the band convergence for the alloy still occurs at high temperature. More generally, the results show that the temperature dependent band shifts make a non-negligible contribution to the band gap in the $Mg_2(Si,\ Sn)$ thermoelectric system. This provides a further avenue for optimization of the TE performance of this material for application under different operating conditions as well as emphasizing the importance of considering temperature dependent band shifts in band structure engineering of prospective TE materials.

ACKNOWLEDGMENTS

This work was supported by National Natural Science Foundation of China (Grants No. 12074241, No. 11929401, and No. 52120204), National Key Research and Development Program of China (Grant No. 2021YFB3502200), Key Research Project of Zhejiang Lab (Grant No. 2021PE0AC02), and Science and Technology Commission of Shanghai Municipality (Grants No. 22XD1400900, No. 20501130600, No. 21JC1402700, and No. 21JC1402600), Shanghai Technical Service Center of Science and Engineering Computing, Shanghai University.

[1] Q. Yang, S. Yang, P. Qiu, L. Peng, T.-R. Wei, Z. Zhang, X. Shi, and L. Chen, Flexible thermoelectrics based on ductile semiconductors, Science **377**, 854 (2022).

[2] H. J. Goldsmid, *Thermoelectric Refrigeration* (Springer, Boston, 1964).

[3] G. Mahan, B. Sales, and J. Sharp, Thermoelectric materials: New approaches to an old problem, Phys. Today **50**(3), 42 (1997).

[4] G. Tan, L. D. Zhao, and M. G. Kanatzidis, Rationally designing high-performance bulk thermoelectric materials, Chem. Rev. **116**, 12123 (2016).

[5] J. Yang, L. Xi, W. Qiu, L. Wu, X. Shi, L. Chen, J. Yang, W. Zhang, C. Uher, and D. J. Singh, On the tuning of electrical and thermal transport in thermoelectrics: An integrated theory–experiment perspective, npj Comput. Mater. **2**, 15015 (2016).

[6] G. S. Nolas, D. T. Morelli, and T. M. Tritt, Skutterudites: A phononglass-electron crystal approach to advanced thermoelectric energy conversion applications, Annu. Rev. Mater. Sci. **29**, 89 (1999).

[7] A. Ali, P. Shamberger, and S. Vaddiraju, Thermal conductivity of $Mg_2Si_{1-x}Sn_x$ nanowire assemblies synthesized using solid-state phase transformation of silicon nanowires, Mater. Res. Express **8**, 025005 (2021).

[8] Y. Wu, W. Xia, W. Gao, W. Ren, and P. Zhang, Engineering the near-edge electronic structure of SnSe through strains, Phys. Rev. Appl. **8**, 034007 (2017).

[9] L. E. Bell, Cooling, heating, generating power, and recovering waste heat with thermoelectric systems, Science **321**, 1457 (2008).

[10] J.-H. Bahk and A. Shakouri, Minority carrier blocking to enhance the thermoelectric figure of merit in narrow-band-gap semiconductors, Phys. Rev. B **93**, 165209 (2016).

[11] R. Freer, D. Ekren, T. Ghosh, K. Biswas, P. Qiu, S. Wan, L. Chen, S. Han, C. Fu, T. Zhu, A. K. M. Ashiquzzaman Shawon, A. Zevalkink, K. Imasato, G. Jeffrey Snyder, M. Ozen, K. Saglik, U. Aydemir, R. Cardoso-Gil, E. Svanidze, R. Funahashi, A. V. Powell, S. Mukherjee, S. Tippireddy, P. Vaqueiro, F. Gascoin, T. Kyratsi, P. Sauerschnig, and T. Mori, Key properties of inorganic thermoelectric materials—tables (version 1), J. Phys. Energy **4**, 022002 (2022).

[12] K. Yin, X. Su, Y. Yan, Y. You, Q. Zhang, C. Uher, M. G. Kanatzidis, and X. Tang, Optimization of the electronic band structure and the lattice thermal conductivity of solid solutions according to simple calculations: A canonical example of the $Mg_2Si_{1-x-y}Ge_xSn_y$ ternary solid solution, Chem. Mater. **28**, 5538 (2016).

[13] W. Liu, X. Tan, K. Yin, H. Liu, X. Tang, J. Shi, Q. Zhang, and C. Uher, Convergence of conduction bands as a means of enhancing thermoelectric performance of n-Type $Mg_2Si_{1-x}Sn_x$ solid solutions, Phys. Rev. Lett. **108**, 166601 (2012).

[14] S.-i. Yi and C. Yu, Variation of thermoelectric figure-of-merits for $Mg_2Si_xSn_{1-x}$ solid solutions, J. Phys. D **54**, 055504 (2021).

[15] W. Liu, X. Tang, H. Li, K. Yin, J. Sharp, X. Zhou, and C. Uher, Enhanced thermoelectric properties of n-type $Mg_{2.16}(Si_{0.4}Sn_{0.6})_{1-y}Sb_y$ due to nanosized Sn-rich precipitates and an optimized electron concentration, J. Mater. Chem. **22**, 13653 (2012).

[16] V. K. Zaitsev, M. I. Fedorov, A. T. Burkov, E. A. Gurieva, I. S. Eremin, P. P. Konstantinov, S. V. Ordin, S. Sano, and M. V. Vedernikov, Some features of the conduction band structure, transport and optical properties of n-type Mg_2Si-Mg_2Sn alloys, in *Proceedings of the XXI International Conference on Thermoelectrics* (IEEE Press, Piscataway, NJ, 2002), pp. 151–154.

[17] W. Yao, S. Hu, F. Jia, J. R. Reimers, Y. Wang, D. J. Singh, and W. Ren, Lattice strain and band overlap of the thermoelectric composite $Mg_2Si_{1-x}Sn_x$, Phys. Rev. B **106**, 104303 (2022).

[18] R. D'Souza, J. D. Querales-Flores, J. Cao, S. Fahy, and I. Savić, Temperature induced band convergence, intervalley scattering, and thermoelectric transport in p-Type PbTe, ACS Appl. Energy Mater. **5**, 7260 (2022).

[19] Y. Pei, X. Shi, A. LaLonde, H. Wang, L. Chen, and G. J. Snyder, Convergence of electronic bands for high performance bulk thermoelectrics, Nature (London) **473**, 66 (2011).

[20] M. Zacharias and F. Giustino, One-shot calculation of temperature-dependent optical spectra and phononinduced band-gap renormalization, Phys. Rev. B **94**, 075125 (2016).

[21] F. Giustino, S. G. Louie, and M. L. Cohen, Electron-phonon renormalization of the direct band gap of diamond, Phys. Rev. Lett. **105**, 265501 (2010).

[22] S. Ponce, Y. Gillet, J. Laflamme Janssen, A. Marini, M. Verstraete, and X. Gonze, Temperature dependence of the electronic structure of semiconductors and insulators, J. Chem. Phys. **143**, 102813 (2015).

[23] F. Giustino, Electron-phonon interactions from first principles, Rev. Mod. Phys. **89**, 015003 (2017).

[24] S. Poncé, G. Antonius, Y. Gillet, P. Boulanger, J. Laflamme Janssen, A. Marini, M. Côté, and X. Gonze, Temperature dependence of electronic eigenenergies in the adiabatic harmonic approximation, Phys. Rev. B **90**, 214304 (2014).

[25] M. Schlüter, G. Martinez, and M. L. Cohen, Pressure and temperature dependence of electronic energy levels in PbSe and PbTe, Phys. Rev. B **12**, 650 (1975).

[26] Z. Wang, J. Xi, J. Ning, K. Guo, B. Duan, J. Luo, G. J. Snyder, J. Yang, and W. Zhang, Temperature-dependent band renormalization in $CoSb_3$ skutterudites due to Sb-ring-related vibrations, Chem. Mater. **33**, 1046 (2021).

[27] J. Park, W. A. Saidi, B. Chorpening, and Y. Duan, Quantifying temperature dependence of electronic band gaps and optical properties in SnO_2 and SnO via first-principles simulations, J. Phys. Chem. C **125**, 22231 (2021).

[28] Y. Huang, J. Zhou, L. Peng, K. Li, S. R. Elliott, and Z. Sun, Antibonding-induced anomalous temperature dependence of the band gap in crystalline $Ge_2Sb_2Te_5$, J. Phys. Chem. C **125**, 19537 (2021).

[29] Z. Zhang, Z. Chen, M. Bouaziz, C. Giorgetti, H. Yi, J. Avila, B. Tian, A. Shukla, L. Perfetti, D. Fan, Y. Li, and A. Bendounan, Direct observation of band gap renormalization in layered indium selenide, ACS Nano **13**, 13486 (2019).

[30] Y.-N. Wu, W. A. Saidi, P. Ohodnicki, B. Chorpening, and Y. Duan, First-principles investigations of the temperature dependence of electronic structure and optical properties of rutile TiO_2, J. Phys. Chem. C **122**, 22642 (2018).

[31] R. Hanus, X. Guo, Y. Tang, G. Li, G. J Snyder, and W. G. Zeier, A chemical understanding of the band convergence in thermoelectric $CoSb_3$ skutterudites: Influence of electron population, local thermal expansion, and bonding interactions, Chem. Mater. **29**, 1156 (2017).

[32] M. Kempa, P. Ondrejkovic, P. Bourges, J. Ollivier, S. Rols, J. Kulda, S. Margueron, and J. Hlinka, The temperature dependence of the phononic band gap of NaI, J. Phys.: Condens. Matter **25**, 055403 (2013).

[33] R. Pässler, Moderate phonon dispersion shown by the temperature dependence of fundamental band gaps of various elemental and binary semiconductors including wide-band gap materials, J. Appl. Phys. **88**, 2570 (2000).

[34] K. P. O'Donnell and X. Chen, Temperature dependence of semiconductor band gaps, Appl. Phys. Lett. **58**, 2924 (1991).

[35] J. Ning, L. Zheng, W. Lei, S. Wang, J. Xi, and J. Yang, Temperature-dependence of the band gap in the all-inorganic perovskite $CsPbI_3$ from room to high temperatures, Phys. Chem. Chem. Phys. **24**, 16003 (2022).

[36] J. Xi, L. Zheng, S. Wang, J. Yang, and W. Zhang, Temperature-dependent structural fluctuation and its effect on the electronic structure and charge transport in hybrid perovskite $CH_{(3)}NH_{(3)}PbI_{(3)}$, J. Comput. Chem. **42**, 2213 (2021).

[37] A. Miglio, V. Brousseau-Couture, E. Godbout, G. Antonius, Y.-.H. Chan, S. G. Louie, M. Côté, M. Giantomassi, and X. Gonze, Predominance of nonadiabatic effects in zero-point renormalization of the electronic band gap, npj Comput. Mater. **6**, 167 (2020).

[38] Y. Zhang, Z. Wang, J. Xi, and J. Yang, Temperature-dependent band gaps in several semiconductors: From the role of electron-phonon renormalization, J. Phys.: Condens. Matter **32**, 475503 (2020).

[39] Z. M. Gibbs, H. Kim, H. Wang, R. L. White, F. Drymiotis, M. Kaviany, and G. J Snyder, Temperature dependent band gap in PbX (X = S, Se, Te), Appl. Phys. Lett. **103**, 262109 (2013).

[40] J. Bhosale, A. K. Ramdas, A. Burger, A. Muñoz, A. H. Romero, M. Cardona, R. Lauck, and R. K. Kremer, Temperature dependence of band gaps in semiconductors: Electron-phonon interaction, Phys. Rev. B **86**, 195208 (2012).

[41] J. Park, W. A. Saidi, J. K. Wuenschell, B. H. Howard, B. Chorpening, and Y. Duan, Assessing the effects of temperature and oxygen vacancy on band gap renormalization in $LaCrO_3$-delta: First-principles and experimental corroboration, ACS Appl. Mater. Interfaces **13**, 17717 (2021).

[42] Y. Tang, Z. M. Gibbs, L. A. Agapito, G. Li, H.-S. Kim, M. Buongiorno Nardelli, S. Curtarolo, and G. J Snyder, Convergence of multi-valley bands as the electronic origin of high thermoelectric performance in $CoSb_3$ skutterudites, Nat. Mater. **14**, 1223 (2015).

[43] W. He, D. Wang, H. Wu, Y. Xiao, Y. Zhang, D. He, Y. Feng, Y.-J. Hao, J.-F. Dong, R. Chetty, L. Hao, D. Chen, J. Qin, Q. Yang, X. Li, J. M. Song, Y. Zhu, W. Xu, C. Niu, X. Li, G. Wang, C. Liu, M. Ohta, S. J. Pennycook, J. He, J. F. Li, and L. D. Zhao, High thermoelectric performance in low-cost $SnS_{0.91}Se_{0.09}$ crystals, Science **365**, 1418 (2019).

[44] J. D. Querales-Flores, J. Cao, S. Fahy, and I. Savić, Temperature effects on the electronic band structure of PbTe from first principles, Phys. Rev. Mater. **3**, 055405 (2019).

[45] A. Togo, L. Chaput, I. Tanaka, and G. Hug, First-principles phonon calculations of thermal expansion in Ti_3SiC_2, Ti_3AlC_2, and Ti_3GeC_2, Phys. Rev. B **81**, 174301 (2010).

[46] G. Kresse and J. Hafner, *Ab initio* molecular dynamics for liquid metals, Phys. Rev. B **47**, 558 (1993).

[47] G. G. Kresse and J. J. Furthmüller, Efficient iterative schemes for *ab initio* total-energy calculations using a plane-wave basis set, Phys. Rev. B **54**, 11169 (1996).

[48] G. Kresse and J. Hafner, *Ab initio* molecular-dynamics simulation of the liquid-metal-amorphous-semiconductor transition in germanium, Phys. Rev. B **49**, 14251 (1994).

[49] P. E. Blochl, Projector augmented-wave method, Phys. Rev. B **50**, 17953 (1994).

[50] H. J. Monkhorst and J. D. Pack, Special points for Brillouin-zone integrations, Phys. Rev. B **13**, 5188 (1976).

[51] A. D. Becke and E. R. Johnson, A simple effective potential for exchange, J. Chem. Phys. **124**, 221101 (2006).

[52] F. Tran and P. Blaha, Accurate band gaps of semiconductors and insulators with a semilocal exchange-correlation potential, Phys. Rev. Lett. **102**, 226401 (2009).

[53] See Supplemental Material at http://link.aps.org/supplemental/10.1103/PhysRevB.108.155205 for information on the EBSs of Mg_2Si, Mg_2Si and $Mg_2Si_{0.375}Sn_{0.625}$ considering LE, VIB, LE+VIB at different temperatures, detailed data of Phonon spectra and expansion coefficient with temperature.

[54] P. Miguel, M. C. de Melo, J. C. de Abreu, B. Guster, M. Giantomassi, Z. Zanolli, X. Gonze, and M. J. Verstraete, High-throughput analysis of Fröhlich-type polaron models, npj Comput. Mater. **9**, 147 (2023).

[55] M. Engel, H. Miranda, L. Chaput, A. Togo, C. Verdi, M. Marsman, and G. Kresse, Zero-point renormalization of the band gap of semiconductors and insulators using the projector augmented wave method, Phys. Rev. B **106**, 094316 (2022).

[56] J.-i. Tani and H. Kido, Lattice dynamics of Mg_2Si and Mg_2Ge compounds from first-principles calculations, Comput. Mater. Sci. **42**, 531 (2008).

[57] A. Kato, T. Yagi, and N. Fukusako, First-principles studies of intrinsic point defects in magnesium silicide, J. Phys.: Condens. Matter **21**, 205801 (2009).

[58] O. Madelung, *Semiconductors: Data Handbook*, 3rd ed. (Springer, Berlin, 2003).

[59] H. Mizoguchi, Y. Muraba, D. C. Fredrickson, S. Matsuishi, T. Kamiya, and H. Hosono, The unique electronic structure of Mg_2Si: Shaping the conduction bands of semiconductors with multicenter bonding, Angew. Chem. Int. Ed Engl. **56**, 10135 (2017).

[60] A. Chernatynskiy and S. R. Phillpot, Anharmonic properties in Mg_2X (X = C, Si, Ge, Sn, Pb) from first-principles calculations, Phys. Rev. B **92**, 064303 (2015).

[61] J. J. Pulikkotil, D. J. Singh, S. Auluck, M. Saravanan, D. K. Misra, A. Dhar, and R. C. Budhani, Doping and temperature dependence of thermoelectric properties in Mg_2(Si, Sn), Phys. Rev. B **86**, 155204 (2012).

[62] P. Boulet and M. C. Record, Influence of the modified Becke-Johnson exchange potential on thermoelectric properties: Application to Mg_2Si, J. Chem. Phys. **135**, 234702 (2011).

[63] M. Y. Au-Yang and M. L. Cohen, Electronic structure and optical properties of Mg_2Si, Mg_2Ge, and Mg_2Sn, Phys. Rev. **178**, 1358 (1969).

[64] V. K. Zaitsev, M. I. Fedorov, E. A. Gurieva, I. S. Eremin, P. P. Konstantinov, A. Yu Samunin, and M.V. Vedernikov, Highly effective $Mg_2Si_{1-x}Sn_x$ thermoelectrics, Phys. Rev. B **74**, 045207 (2006).

[65] F. Karsai, M. Engel, E. Flage-Larsen, and G. Kresse, Electron–phonon coupling in semiconductors within the GW approximation, New J. Phys. **20**, 123008 (2018).

[66] X. Gonze, P. Boulanger, and M. Côté, Theoretical approaches to the temperature and zero-point motion effects on the electronic band structure, Ann. Phys. **523**, 168 (2011).

[67] K. Chang-Eun, S. Aloysius, and S. Catherine, Unraveling the origins of conduction band valley degeneracies in $Mg_2Si_{1-x}Sn_x$ thermoelectrics, Phys. Chem. Chem. Phys. **18**, 939 (2016).

[68] B. Ryu, S. Park, E.-A. Choi, J. de Boor, P. Ziolkowski, J. Chung, and S. D. Park, Hybrid-functional and quasiparticle calculations of band structures of Mg_2Si, Mg_2Ge, and Mg_2Sn, J. Korean Phys. Soc. **75**, 144 (2019).